Andreev quantum dot with several conducting channels

I. A. Sadovskyy, G. B. Lesovik, G. Blatter, T. Jonckheere, and T. Martin

Andreev quantum dot with several conducting channels

I.A. Sadovskyy[1], G.B. Lesovik[2], G. Blatter[3], T. Jonckheere[4], and T. Martin[4]

[1] *Rutgers University, 136 Frelinghuysen Road, Piscataway, New Jersey, 08854, USA*
[2] *L.D. Landau Institute for Theoretical Physics RAS,*
Akademika Semenova av., 1-A, 142432 Chernogolovka, Russia
[3] *Theoretische Physik, Wolfgang-Pauli-Str. 27, ETH-Zurich, CH-8093 Zürich, Switzerland and*
[4] *Centre de Physique Théorique, CNRS UMR 7332,*
Aix-Marseille Université, Case 907, F-13288 Marseille, France
(Dated: March 16, 2012)

We study an Andreev quantum dot, that is a quantum dot inserted in a superconducting ring, with several levels or conducting channels. We analyze the degeneracy of the ground state as a function of the phase difference and of the gate voltage and find its dependence on the Coulomb interaction within and between channels. We compute a (non integer) charge of the dot region and Josephson current. The charge-to-phase and current-to-gate voltage sensitivities are studied. We find that, even in the presence of Coulomb interaction between the channels, the sensitivity increases with the number of channels, although it does not scale linearly as in the case with no interactions. The Andreev quantum dot may therefore be used as a sensitive detector of magnetic flux or as a Josephson transistor.

PACS numbers: 74.78.Na, 73.21.La, 74.45.+c

I. INTRODUCTION

In the middle of the last century, Josephson showed that a non dissipative current can flow between two superconductors separated by an intermediate region when a phase difference is applied between the two superconductors.[1–3] This intermediate region can, in practice, be composed of an insulator, a normal metal, a constriction, etc. Recent developments of nanotechnology allow to insert quantum dots, e.g., using carbon nanotubes[4,5] in this region. These types of Josephson junctions are called Andreev quantum dots.[6,7] The charge of the Andreev dot was shown to vary smoothly with the phase difference between the superconductors[7,8] in the absence of Coulomb interaction.

Ref. 7 showed that the charge could be tuned continuously from 0 to $2e$ depending on the phase difference φ and gate voltage V_g. In Refs. 9,10 it was shown that the Coulomb interaction can change the property of the ground state, from a usual non-degenerate state with two quasi-particles to a doubly degenerate state with one quasi-particle. The present article is a logical continuation of the above-mentioned work and is devoted to the case of several channels. These channels may appear due to the presence of two orbits in a single-wall carbon nanotubes and in multi-wall nanotubes[11], or due to an inhomogeneous distribution of transverse quantized energy levels in metal wires.[12] In this article, we answer the natural question: how is the charge dependence on the phase difference affected by the presence of such channels, what is the effect of Coulomb interaction between channels, and how is does this dependence scale with the number of channels. The calculation is done in the limit of a large superconducting gap.

We describe the ground state properties for different setups with different strengths of the regular An-

dreev reflection (AR)[13] and crossed Andreev reflection (CAR)[14–17] for different types of Coulomb interaction, such as metal nanowires with 1 channel, single-wall carbon nanotubes (SWNT) with 2 orbital channels, multi-wall carbon nanotubes (MWNT) with 4 channels, and two separate SWNTs with 2×2 channels. In this article, we mainly focus on the dependencies on the tunable parameters gate voltage and superconducting phase difference. We consider the interplay between phase-sensitive singlet (non-degenerate) and phase-insensitive doubled (doubly degenerate) states from different channels, study the current-to-gate voltage and charge-to-phase sensitivities, and discuss two applications, the Josephson transistor[18] and a magnetometer based on an Andreev quantum dot.[10]

In Sec. II, we describe a setup based on a quantum dot with several levels or alternatively an intermediate region composed of several single-wall nanotubes/a multi-wall nanotube. The model Hamiltonian is introduced in Sec. III. In Sec. IV, we represent the iterative scheme providing the matrix elements of the N-channel Hamiltonian. Using these results, we study the degeneracy and
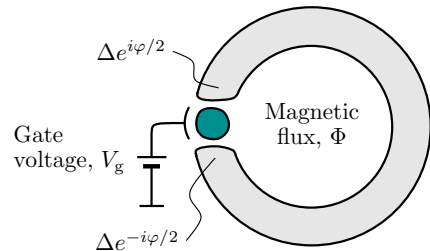

FIG. 1: Josephson junction inserted into a superconducting loop which is driven by an external magnetic flux Φ and gate voltage V_g.

energy of the ground state as a function of the superconducting phase difference and gate voltage in Sec. V. Furthermore, we analyze the magnetic properties of the dot in Sec. VI. The charge on the dot and the Josephson current are calculated in Sec. VII and their "sensitivities" are discussed in Sec. VIII.

II. SETUP

As shown in Fig. 1 the setup consists of a structured Josephson junction in the form of an Andreev quantum dot inserted into a superconducting loop. We consider a quantum dot with one or several conducting channels and account for the Coulomb interaction and crossed Andreev reflection. In the Andreev dot without Coulomb interactions, strong normal reflection (electron $\rightarrow$ electron, hole $\rightarrow$ hole) competes with Andreev reflection (electron $\rightarrow$ hole, hole $\rightarrow$ electron) and as a result a strong dependence of the charge and current on the superconducting phase difference occurs. Every conducting channel contributes to the charge[7] and current.[18,19] Our Andreev dots describe a situation where the resonance width Γ is much smaller than the superconducting gap Δ ($\Gamma \ll \Delta$) and the length of the normal part L is much shorter than the superconducting coherence length ξ ($L \ll \xi$). The superconducting phase difference φ across the junction is controlled by the magnetic flux Φ passing through the ring: $\varphi = 2\pi\Phi/\Phi_0$, where Φ_0 is the flux quantum $\Phi_0 = 2|e|/2\pi\hbar$ and $e = -|e|$ is a charge of one electron.

Realistic experimental setups might be based on a single-wall nanotube,[4,5] on two or more single-wall nanotubes placed in parallel, or on a multi-wall nanotube. The case with two parallel single-wall nanotubes is illustrated in Fig. 2(b): this case is interesting because the Coulomb interaction between nanotubes can be smaller than in each nanotube. If such nanotubes are separated by a large distance, the effects of the tubes will be additive. The second interesting and experimentally realized case is the multi-wall nanotube with approximately equal interactions in each channel and between them, as depicted in Fig. 2(c).

III. MODEL

We consider a SWNT suspended between two superconducting leads, cf. Fig. 2(a). Additional gates placed above the nanotube allow to define precisely the extent of the quantum dot and therefore allow to modulate its energy levels. An overall gate voltage allows to apply an electric field to the entire structure and changes the position of the normal dot levels ε_i (index $i = 1, \ldots, N$ labels the channels). The normal island(s) can be described as zero dimensional objects.

The model can be described by a Hamiltonian which includes the dot and its internal degrees of freedom, the leads, and the tunnel coupling between the latter two, $\hat{H} = \hat{H}_\mathrm{D} + \hat{H}_\mathrm{S} + \hat{H}_\mathrm{T}$. The first part $\hat{H}_\mathrm{D}$ describes the quantum dot with N normal levels

$$\hat{H}_\mathrm{D} = \sum_{i=1}^{N} \varepsilon_i \hat{n}_i + \sum_{i,j=1}^{N} U_{ij} \hat{n}_i \hat{n}_j, \qquad (1)$$

where the first term represents the interaction with the external gate, $\hat{n}_i = \hat{n}_{i\uparrow} + \hat{n}_{i\downarrow}$, $\hat{n}_{i\sigma} = \hat{d}_{i\sigma}^\dagger \hat{d}_{i\sigma}$, and $\hat{d}_{i\sigma}^\dagger$ and $\hat{d}_{i\sigma}$ are electronic creation and annihilation operators for the ith level in the dot; $\sigma = \uparrow, \downarrow$, and ε_i is the ith energy level with respect to the Fermi level. The second term describes the Coulomb interaction within the channels (U_{ii}) and between different channels (U_{ij}, $i \neq j$). The symmetric matrix U_{ij} is positive definite and all its elements are positive.[20] The lead Hamiltonian describes two BCS superconductors [with a lead index $\ell = \mathrm{L}, \mathrm{R}$ (left, right)]

$$\hat{H}_\mathrm{S} = \sum_{\ell,k} \hat{\Psi}_{\ell,k}^\dagger (\xi_k \hat{\sigma}_z + \Delta\hat{\sigma}_x) \hat{\Psi}_{\ell,k}, \quad \hat{\Psi}_{\ell,k} = \begin{bmatrix} \psi_{\ell,k,\uparrow} \\ \psi_{\ell,-k,\downarrow}^\dagger \end{bmatrix} \quad (2)$$

with an energy dispersion in the superconducting leads $\xi_k = \hbar^2 k^2/2m - E_\mathrm{F}$ and an absolute value of the gap Δ in the bulk of the superconductors. The electron hopping term between dots and leads is given by

$$\hat{H}_\mathrm{T} = \sum_{\ell,k} (\hat{\Psi}_{\ell,k}^\dagger \hat{\mathcal{T}}_\ell \hat{d} + \mathrm{H.c.}), \quad \hat{d} = \begin{bmatrix} \hat{d}_\uparrow \\ \hat{d}_\downarrow^\dagger \end{bmatrix}, \qquad (3)$$

where $\hat{\mathcal{T}}_{\mathrm{L},\mathrm{R}} = t_{\mathrm{L},\mathrm{R}} \hat{\sigma}_z e^{\pm i \hat{\sigma}_z \varphi/4}$ and t_ℓ are tunneling amplitudes between the superconductors and the dot. The superconductor has a phase $\varphi/2$ on the left and $-\varphi/2$ on the right. The calculation of observables for a thermal equilibrium system starts from the evaluation of the partition function $Z = \mathrm{Tr}\{e^{-\beta\hat{H}}\}$, where β is the inverse temperature.

We work in the limit of a large superconducting gap $|\varepsilon_i|, U_{ij}, \Gamma_{ij} \ll \Delta$ (the so-called $\Delta \rightarrow \infty$ limit), where Γ_{ij} are the resonance half-widths originating from tunneling processes (3). In this limit, one can integrate over the lead degrees of freedom and benefit from the absence of retardation effects due to the latter. The Hamiltonian $\hat{H}$ can be rewritten in a simpler form

$$\hat{\mathcal{H}}_N = \sum_{i=1}^{N} \varepsilon_i(V_\mathrm{g}) \hat{n}_i + \sum_{i,j=1}^{N} U_{ij} \hat{n}_i \hat{n}_j$$
$$+ \sum_{i,j=1}^{N} \tilde{\Gamma}_{ij}(\varphi) [\hat{d}_{i\downarrow} \hat{d}_{j\uparrow} + \mathrm{H.c.}], \qquad (4)$$

describing the dot alone with the superconductors defining the boundary conditions.[21–23] We explicitly indicate the number of channels N in the Hamiltonian $\hat{\mathcal{H}}_N$ Eq. (4) and build an iterative scheme for its matrix elements $\mathcal{H}_N$ on N. Upon integration, Eqs. (2) and (3) generate the
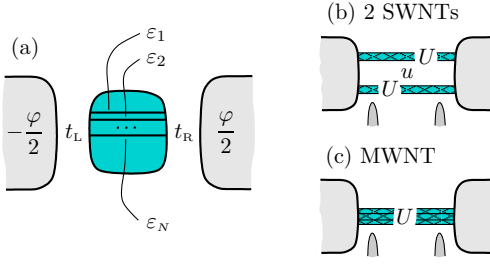
FIG. 2: Structure of the Andreev quantum dot with N channels. (a) A dot with N normal levels with corresponding energies $\varepsilon_1, \ldots, \varepsilon_N$ is inserted between two superconductors with phase difference φ across the tunnel junctions t_{L} and t_{R}. (b) Quantum dot system based on two parallel single-wall nanotubes. The barriers t_{L} and t_{R} are formed by two external gates. The Coulomb interaction u between the channels may be smaller than the interaction U inside a given channel. (c) Quantum dot based on a multi-wall nanotube. The Coulomb energy between orbital channels is approximately equal to the ones inside each channel.

last term in Eq. (4), which implies that this Hamiltonian does not conserve the number of electrons. The coefficients $\tilde{\Gamma}_{ij}$ are directly derived from the tunneling amplitudes $t_{\mathrm{L,R}}$ and describe two-particle tunneling processes involving both Andreev and normal scattering events at the left and right boundaries. For symmetric boundaries with equal transparencies $|t_{\mathrm{L}}|^2 = |t_{\mathrm{R}}|^2 = |t|^2$ we find $\tilde{\Gamma}_{ij} = \Gamma_{ij} \cos(\varphi/2)$. The symmetric matrix Γ_{ij} describes Andreev reflection, the annihilation of two quasiparticles from the ith and j^{th} channel $\hat{d}_{i\downarrow}\hat{d}_{j\uparrow}$ (with simultaneous creation of a Cooper pair in the superconductor) and the opposite process. The diagonal terms $\tilde{\Gamma}_{ii}$ correspond to the regular Andreev reflection inside i^{th} channel, the off-diagonal terms $\tilde{\Gamma}_{ij}, (i \neq j)$ describes the crossed Andreev reflection (CAR) between the ith and j^{th} channel. The element Γ_{ij} can be treated as the resonance half-width of the normal tunneling process between the ith and j^{th} channel. Note that for a diagonal matrix Γ_{ij} and U_{ij} (with $\Gamma_{ij} = 0$, $U_{ij} = 0$, $i \neq j$) the channels are additive and the answers for all physical quantities can be obtained by summation over all channels.

IV. ITERATIVE SCHEME

The Hamiltonian Eq. (4) for a single channel (the first channel in the iterative scheme presented below) has the following form

$$\hat{H}_1 = \varepsilon_1 \hat{n}_1 + U_1 \hat{n}_1^2 + \tilde{\Gamma}_1 [\hat{d}_{1\downarrow}\hat{d}_{1\uparrow} + \mathrm{H.c.}], \qquad (5)$$

where the $\hat{n}_{1\sigma}^2$ contributions from the sum $\hat{n}_1^2 = (\hat{n}_{1\uparrow} + \hat{n}_{1\downarrow})^2$ has been absorbed in a shift of ε_1. We denote the Hamiltonian of the ith channel as $\hat{H}_i$ and the total Hamiltonian of N channels as $\hat{\mathcal{H}}_N$. The corresponding matrix of the H_1 Hamiltonian has dimension 4×4 and can be calculated in a basis of four states $|\nu\rangle_1 = \{|0\rangle_1,$

$|\uparrow\rangle_1, |\downarrow\rangle_1, |2\rangle_1\}$, the state with no electrons $|0\rangle$, with one electron with spin up $|\uparrow\rangle = \hat{d}_{\uparrow}^{\dagger}|0\rangle$ or spin down $|\downarrow\rangle = \hat{d}_{\downarrow}^{\dagger}|0\rangle$, and the two electron state $|2\rangle = \hat{d}_{\uparrow}^{\dagger}\hat{d}_{\downarrow}^{\dagger}|0\rangle$

$$H_1 = \varepsilon_1 n_1 + U_1 n_1^2 + \mathrm{adiag}_1\{\tilde{\Gamma}_1, 0, 0, \tilde{\Gamma}_1\}$$

$$= \begin{bmatrix} 0 & 0 & 0 & \tilde{\Gamma}_1 \\ 0 & \varepsilon_1 + U_1 & 0 & 0 \\ 0 & 0 & \varepsilon_1 + U_1 & 0 \\ \tilde{\Gamma}_1 & 0 & 0 & 2\varepsilon_1 + 4U_1 \end{bmatrix}_1, \qquad (6)$$

where

$$n_1 = n_{1\uparrow} + n_{1\downarrow} = Q_1/e = \mathrm{diag}_1\{0, 1, 1, 2\} \qquad (7)$$

are matrix elements of the dimensionless charge operator and $\hat{Q}_1 = e\hat{n}_1$. In what follows, the expression $\mathrm{adiag}\{x_1, x_2, \ldots, x_N\}$ stands for the $N \times N$ matrix A_{ij}, where $A_{i,N-i+1} = x_i$ and $A_{i,j} = 0$ for $j \neq N-i+1$. The eigenvalues of Eq. (6) can be easily calculated. They consist of two non-degenerate levels with energies

$$E_{0/2} = \varepsilon_1 + 2U_1 \mp \sqrt{(\varepsilon_1 + 2U_1)^2 + \tilde{\Gamma}_1^2} \qquad (8)$$

and a doubly degenerate level with energy

$$E_1 = \varepsilon_1 + U_1 \qquad (9)$$

which can be split into two separate levels by an external magnetic field through the Zeeman effect. Usually, the ground state of the Hamiltonian Eq. (6) is given by the singlet E_0. But in the case of nonzero Coulomb interaction $U_1 > 0$ there exists a range of parameters φ and ε_i for which the ground state is doubly degenerate with energy E_1. The doublet region is defined by the inequality

$$(\varepsilon_1 + 2U_1)^2 + \tilde{\Gamma}_1^2 < U_1^2, \qquad (10)$$

where $\tilde{\varepsilon} = \varepsilon_1 + 2U_1$. For an asymmetric dot ($|t_{\mathrm{L}}| \neq |t_{\mathrm{R}}|$), in the presence of electron-phonon interaction or other perturbations, the "critical" U_1 is different from zero, $U_{1,\mathrm{C}} > 0$.[10] In this article, we ignore such non-idealities and concentrate on the simplest case. The same results are valid for any other $i > 1$ channel; they can be obtained by the substitution $\varepsilon_1 \to \varepsilon_i$, $\Gamma_1 \to \Gamma_i$, and $U_1 \to U_i$.

The structure of the ground state in the one-channel case is presented in Fig. 3 as a function of phase φ and the "central" dot-level $\tilde{\varepsilon} = \varepsilon_1 + 2U_1$. The blue figures in the center represent the doublet state (9), their shapes are defined by the inequality (10), the white space around corresponds to a usual singlet state with energy (8). For two completely separated single-channel dots with the same levels $\varepsilon_1 = \varepsilon_2$ connected in parallel, the dependence is the same, however, now the central figure corresponds to a four-fold degenerate situation.

We now go back to the N-channel case. We calculate the matrix elements of the Hamiltonian Eq. (4) in
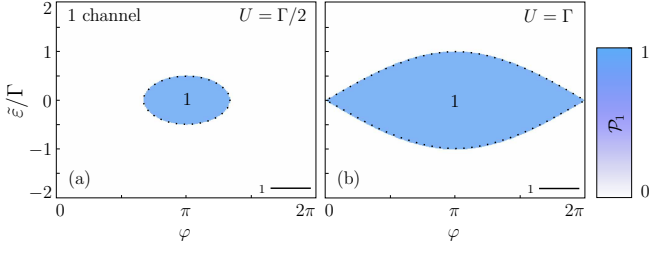
FIG. 3: System degeneracy $\mathcal{P}_1$ in the ground state in $(\varphi, \tilde{\varepsilon})$ space for the channel $N = 1$.

the basis $|\nu\rangle_1 \otimes |\nu\rangle_2 \otimes \ldots \otimes |\nu\rangle_N = \{|0,\ldots,0\rangle, |0,\ldots,\uparrow\rangle, |0,\ldots,\downarrow\rangle,\ldots, |2,\ldots,\downarrow\rangle, |2,\ldots,2\rangle\}$, where $|\nu\rangle_i = \{|0\rangle_i, |\uparrow\rangle_i, |\downarrow\rangle_i, |2\rangle_i\}$ are states of the Hamiltonian for the single channel case Eq. (6)

$$\hat{\mathcal{H}}_N = \sum_{i=1}^{N} \mathbb{1}_1 \otimes \ldots \otimes \hat{H}_i \otimes \ldots \otimes \mathbb{1}_N \qquad (11)$$

$$+ \sum_{\substack{i,j=1 \\ i \neq j}}^{N} U_{ij} \, \mathbb{1}_1 \otimes \ldots \otimes \hat{n}_i \otimes \ldots \otimes \hat{n}_j \otimes \ldots \otimes \mathbb{1}_N$$

$$+ \sum_{\substack{i,j=1 \\ i \neq j}}^{N} \tilde{\Gamma}_{ij} \Big[\mathbb{1}_1 \otimes \ldots \otimes \hat{d}_{i\downarrow} \otimes \ldots \otimes \hat{d}_{j\uparrow} \otimes \ldots \otimes \mathbb{1}_N$$

$$+ \mathbb{1}_1 \otimes \ldots \otimes \hat{d}^\dagger_{j\uparrow} \otimes \ldots \otimes \hat{d}^\dagger_{i\downarrow} \otimes \ldots \otimes \mathbb{1}_N \Big].$$

Here, the first sum takes into account the interactions inside each channel (given by the direct tensor product of H_i's and unity operators $\mathbb{1}_j$ in the other subspaces). The second sum is the interaction between channels, each term represents the tensor product of the charge operator in the ith channel and in the jth channel [as given by Eq. (7)]. Here, $\mathbb{1}_i$ is the unit matrix in the Hilbert subspace of the ith channel and Q_i is the matrix characterizing the ith channel charge. The third sum describes CAR; each term corresponds to the CAR in the ith and j^{th} channels. The Coulomb interaction inside each channel and the regular Andreev reflection are accounted for in the first term.

Let us construct a recursive procedure in N for the matrix elements corresponding to the N-channel Hamiltonian. As the initial step of the recursion $N = 1$ we take the matrix (6). At the second step $N = 2$ we build a matrix in $|\nu\rangle_1 \otimes |\nu\rangle_2$ in the following way:

$$\mathcal{H}_2 = \text{diag}_2\{H_1, H_1 + \varepsilon_2 + U_2 + \mathbb{U}_{21}, H_1 + \varepsilon_2 + U_2 + \mathbb{U}_{21},$$
$$H_1 + 2\varepsilon_2 + 4U_2 + \mathbb{U}_{22}\} \qquad (12)$$

$$+ \tilde{\Gamma}_2 \begin{bmatrix} 0 & 0 & 0 & \mathbb{1}_1 \\ 0 & 0 & 0 & 0 \\ 0 & 0 & 0 & 0 \\ \mathbb{1}_1 & 0 & 0 & 0 \end{bmatrix}_2 + \tilde{\Gamma}_{12} \begin{bmatrix} 0 & d^\dagger_{1\downarrow} & d^\dagger_{1\uparrow} & 0 \\ d_{1\downarrow} & 0 & 0 & -d^\dagger_{1\uparrow} \\ d_{1\uparrow} & 0 & 0 & d^\dagger_{1\downarrow} \\ 0 & -d_{1\uparrow} & d_{1\downarrow} & 0 \end{bmatrix}_2 ,$$

where we keep in mind that $\tilde{\Gamma}_{12} = \tilde{\Gamma}_{21}$. The matrices

$$d_{i\uparrow} = \begin{bmatrix} 0 & 0 & 0 & 0 \\ 1 & 0 & 0 & 0 \\ 0 & 0 & 0 & 0 \\ 0 & 0 & 1 & 0 \end{bmatrix}_i , \qquad d_{i\downarrow} = \begin{bmatrix} 0 & 0 & 0 & 0 \\ 0 & 0 & 0 & 0 \\ 1 & 0 & 0 & 0 \\ 0 & -1 & 0 & 0 \end{bmatrix}_i$$

and the corresponding Hermitian conjugates $d^\dagger_{i\uparrow}, d^\dagger_{i\downarrow}$ are the matrix elements of the operators $\hat{d}_{i\uparrow}, \hat{d}_{i\downarrow}$ and $\hat{d}^\dagger_{i\uparrow}, \hat{d}^\dagger_{i\downarrow}$ in the ith channel basis. This is a 16×16 matrix (the Hilbert space of the 1st channel with dimension 4 should be multiplied by the Hilbert space of the 2nd one with the same dimension). Each "element" is a 4×4 block, "diag" and "adiag" to be in the 2nd channel subspace. H_1 originates from Eq. (6), with scalar elements to be multiplied by $\mathbb{1}_1$. The matrices $\mathbb{U}_{21} = \text{diag}_1\{0, 0, 0, 8U_{12}\}$ and $\mathbb{U}_{22} = \text{diag}_1\{0, 8U_{12}, 8U_{12}, 0\}$ are based on the term U_{12} which is responsible for the interaction between channels. For the noninteracting case $U_{12} = 0$, the structure of the ground state is presented in Fig. 4(a) $[\varepsilon_2 - \varepsilon_1 = 0]$ and 4(d) $[\varepsilon_2 - \varepsilon_1 = \Gamma]$ in coordinates $(\varphi, \tilde{\varepsilon})$, where $\tilde{\varepsilon} = (\varepsilon_1 + \varepsilon_2)/2 + U_1 + U_2$ is the average and renormalized normal level in the dot. The interacting case is shown in Figs. 4(g) and 4(j), where $\tilde{\varepsilon} = (\varepsilon_1 + \varepsilon_2)/2 + U_1 + U_2 + 2U_{12}$; see Sec. V for more details.

In the same way we can write a recursive formula for $\mathcal{H}_N$. The easiest way to write it down is

$$\mathcal{H}_N = \sum_{i=1}^{N} \varepsilon_i n_i + \sum_{i=1}^{N} U_i n_i^2 + \sum_{i=1}^{N} \tilde{\Gamma}_i \, \text{adiag}_i\{1, 0, 0, 1\}$$
$$+ \sum_{\substack{i,j=1 \\ i \neq j}}^{N} U_{ij} n_i n_j + \sum_{\substack{i,j=1 \\ i \neq j}}^{N} \tilde{\Gamma}_{ij} \big[d_{i\downarrow} d_{j\uparrow} + d^\dagger_{j\uparrow} d^\dagger_{i\downarrow} \big]. \qquad (13)$$

Here each matrix with index i should be written as a matrix of size $4^i \times 4^i$ (i.e., in the subspace of the ith channel). Herein each element of the matrix associated with the ith channel is multiplied by a unitary matrix of size $4^{i-1} \times 4^{i-1}$ and starts on column $(c-1)2^{i-1}+1$ and on row $(r-1)2^{i-1}+1$ of the total matrix, where $c = 1,\ldots,4$ is the column and $r = 1,\ldots,4$ is the row in the original 4×4 matrix of the ith channel. Schematically the recursive procedure for building the N-channel matrix can be represented as (for $N = 3$)

$$\begin{bmatrix} \begin{bmatrix} \begin{bmatrix} \cdot \end{bmatrix}_1 & \cdots & \begin{bmatrix} \cdot \end{bmatrix}_1 \\ \vdots & & \vdots \\ \begin{bmatrix} \cdot \end{bmatrix}_1 & \cdots & \begin{bmatrix} \cdot \end{bmatrix}_1 \end{bmatrix}_2 & \cdots & \begin{bmatrix} \begin{bmatrix} \cdot \end{bmatrix}_1 & \cdots & \begin{bmatrix} \cdot \end{bmatrix}_1 \\ \vdots & & \vdots \\ \begin{bmatrix} \cdot \end{bmatrix}_1 & \cdots & \begin{bmatrix} \cdot \end{bmatrix}_1 \end{bmatrix}_2 \\ \vdots & & \vdots \\ \begin{bmatrix} \begin{bmatrix} \cdot \end{bmatrix}_1 & \cdots & \begin{bmatrix} \cdot \end{bmatrix}_1 \\ \vdots & & \vdots \\ \begin{bmatrix} \cdot \end{bmatrix}_1 & \cdots & \begin{bmatrix} \cdot \end{bmatrix}_1 \end{bmatrix}_2 & \cdots & \begin{bmatrix} \begin{bmatrix} \cdot \end{bmatrix}_1 & \cdots & \begin{bmatrix} \cdot \end{bmatrix}_1 \\ \vdots & & \vdots \\ \begin{bmatrix} \cdot \end{bmatrix}_1 & \cdots & \begin{bmatrix} \cdot \end{bmatrix}_1 \end{bmatrix}_2 \end{bmatrix}_3$$

The smallest "rectangle" corresponds to the Hamiltonian H_1. In a second step, we insert such blocks in the Hamiltonian H_2 and continue the procedure till N. At each
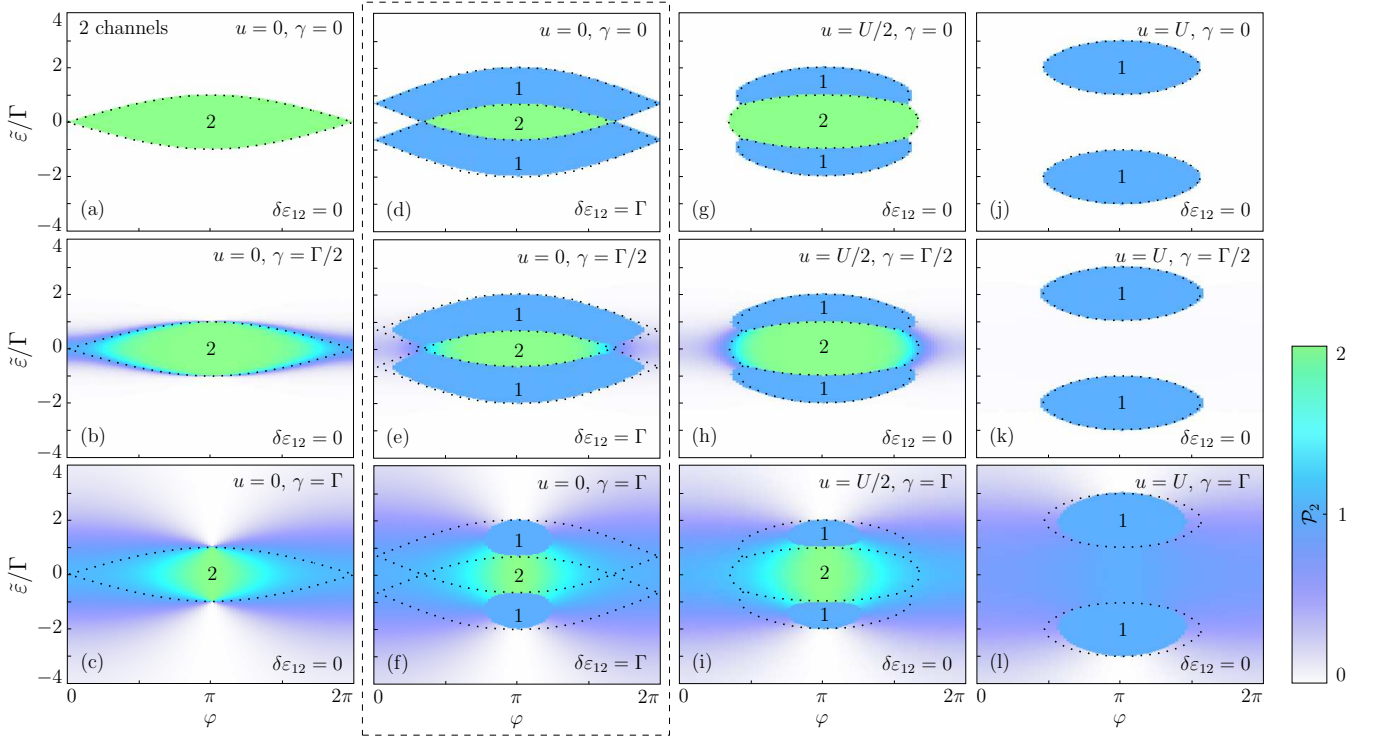
FIG. 4: System degeneracy $\mathcal{P}_2$ in the ground state in the $(\varphi, \tilde{\varepsilon})$ space for $N = 2$ channels. The Coulomb matrix U_{ij} is defined by Eq. (16), CAR is defined by Eq. (17). The Coulomb interaction inside each channel is equal and equal to the resonance width, $U = \Gamma$. The Coulomb interaction between channels varies from left [$u = 0$ in (a)-(c)] to right [$u = U$ in (j)-(l)]; The CAR parameter varies from top [$\gamma = 0$ in (a), (d), (g), and (j)] to bottom [$\gamma = \Gamma$ in (c), (f), (i), and (l)]. The difference in dot levels $\delta\varepsilon_{12} = \varepsilon_2 - \varepsilon_1 = \Gamma$ in (d)-(f) and $\delta\varepsilon_{12} = 0$ in all other plots. (a) In the non-interacting case the degenerate region with $\mathcal{P}_2 = 2$ (green) inside the non-degenerate region $\mathcal{P}_2 = 0$ (white) is defined by the inequality (10) and coincides with the same region of each channel. (b) and (c) CAR smears the border and $\mathcal{P}_2$ goes from 0 to 2 continuously. (c) Two doubly-degenerate regions (blue) shifted by $\delta\varepsilon_{12}$; the intersection represents a fourth-fold degenerate region (green). (e) and (f) The border is (non-uniformly) smeared due to CAR, starting from the point where three regions with $\mathcal{P}_2 = 0$, 1, and 2 join together and ending with a smeared four-fold region. (g)-(i) The average Coulomb interaction between the channels $u = U/2$ separates apart the region with $\mathcal{P}_2 = 1$ in (a) by the distance $4u$, but in a different manner from (b); CAR smears the borders of the $\mathcal{P}_2 = 2$ region and diminishes the $\mathcal{P}_2 = 1$ regions. (j)-(l) The maximal Coulomb interaction between channels $u = U$ totally splits the $\mathcal{P}_2 = 2$ region into two regions with $\mathcal{P}_2 = 1$ (the distance is still $4u$); CAR slowly increases $\mathcal{P}_2$ from 0 to 1 and slightly reduces the $\mathcal{P}_2 = 1$ regions.

i^{th} step, we multiply the current space by the Hilbert subspace of the ith Andreev level.

Note that the same procedure can be realized by using the Bogoliubov-de Gennes equations and the scattering matrix approach in the tunneling regime (with a transparency of each junction much less than unity) as was done in Ref. 10 for a single channel. However, this approach is poorly scalable with N and the calculation is much more cumbersome. See also Ref. 24 for the correspondence between the tunneling Hamiltonian method and the scattering matrix approach.

In the present notation, the first, the second, and the fourth sum in Eq. (13) are diagonal. In the absence of superconductivity they define energy levels of the system and the Coulomb interaction leads to level "repulsion". The third term of Eq. (13) includes the dependence on the superconducting phase difference and mixes the states due to presence of Cooper pairs in the super-

conductors. At $\varphi = \pi$ the Hamiltonian Eq. (13) is diagonal and its eigenvalues can be found analytically.
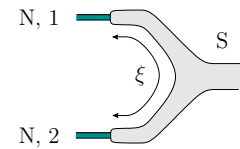

FIG. 5: The Crossed Andreev reflection between channels 1 and 2 in the fork (or Y) geometry is suppressed if the length between the NS interfaces is much larger then the coherence length ξ.
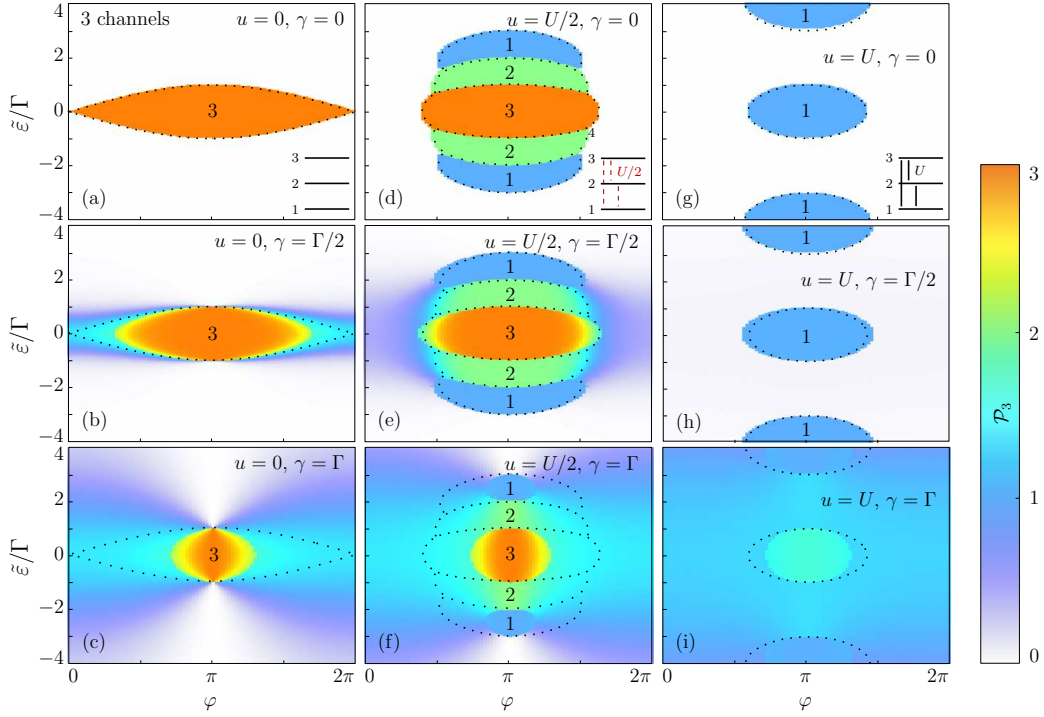
FIG. 6: System degeneracy $\mathcal{P}_3$ of the ground state for $N = 3$ channels; the same as in Figs. 4(a)-4(c), 4(g)-4(i), and 4(j)-4(l).

V. ENERGY LEVELS AND DEGENERACIES

In the single channel case, the ground state is formed by non-degenerate [Eq. (8)] or doubly degenerate [Eq. (9)] levels. However, for a large number of channels one can expect to observe $2^{\mathcal{P}_N}$ degeneracy, where $\mathcal{P}_N$ is the number of Andreev levels in the doublet state.

To characterize the state of each channel let us first determine the operator

$$\hat{p}_i = \mathrm{diag}_i\{0, 1, 1, 0\} \tag{14}$$

which is defined in the Hilbert space of the ith channel. For the case with no interaction, this operator defines the p_i value equal to 0 if the ith channel is in the singlet state and 1 if the ith channel is in the doublet state. In the case including interaction, p_i may vary from 0 to 1. The $\mathcal{P}_N$ value of the operator

$$\hat{\mathcal{P}}_N = \sum_{i=1}^{N} \mathbb{1}_1 \otimes \ldots \otimes \hat{p}_i \otimes \ldots \otimes \mathbb{1}_N \tag{15}$$

characterizes the state of the entire system, $0 \leqslant \mathcal{P}_N \leqslant N$. In the non-interacting case $\mathcal{P}_N$ gives the number of channels in doublet states and can be considered as the degeneracy of the ground state.

In addition, the mechanism for intra-state transitions with different $\mathcal{P}_N$ should be discussed. As mentioned above these transitions qualitatively change the properties of the system, the charging effects, the transport properties, and the magnetic response to the external field. Such transitions occur, for instance, due to electron-phonon interactions involving a continuous spectrum.[7] Their rate is suppressed by the exponential factor $e^{-\Delta/k_{\text{B}}\Theta}$, where k_{B} and Θ are the Boltzmann constant and temperature, respectively.[6,7] Thus, transitions where the system's spin changes by $1/2$ are more rare than transitions where the spin remains unchanged. Therefore, the above picture for conversion between singlet and doublet in one channel is valid for an adiabatically slow change of the parameters φ and $\tilde{\varepsilon}$.

Let us consider cases defined by different matrices U_{ij} and Γ_{ij}. The diagonal elements of the Coulomb matrix U_{ij} define the interaction in each channel. The off-diagonal elements describing the interactions between channels can be of the order of the diagonal elements for the multi-channel wire and about zero for a few separated wires. We can vary the "ratio" between off-diagonal to diagonal elements from 0 to 1. In the same way, we can vary the off-diagonal elements of Γ_{ij}, which are of the order of the diagonal elements and about zero for separated channels, e.g., see the superconductor in fork geometry in Fig. 5.

A. Toy model

We parametrize the Coulomb interaction matrix with two parameters

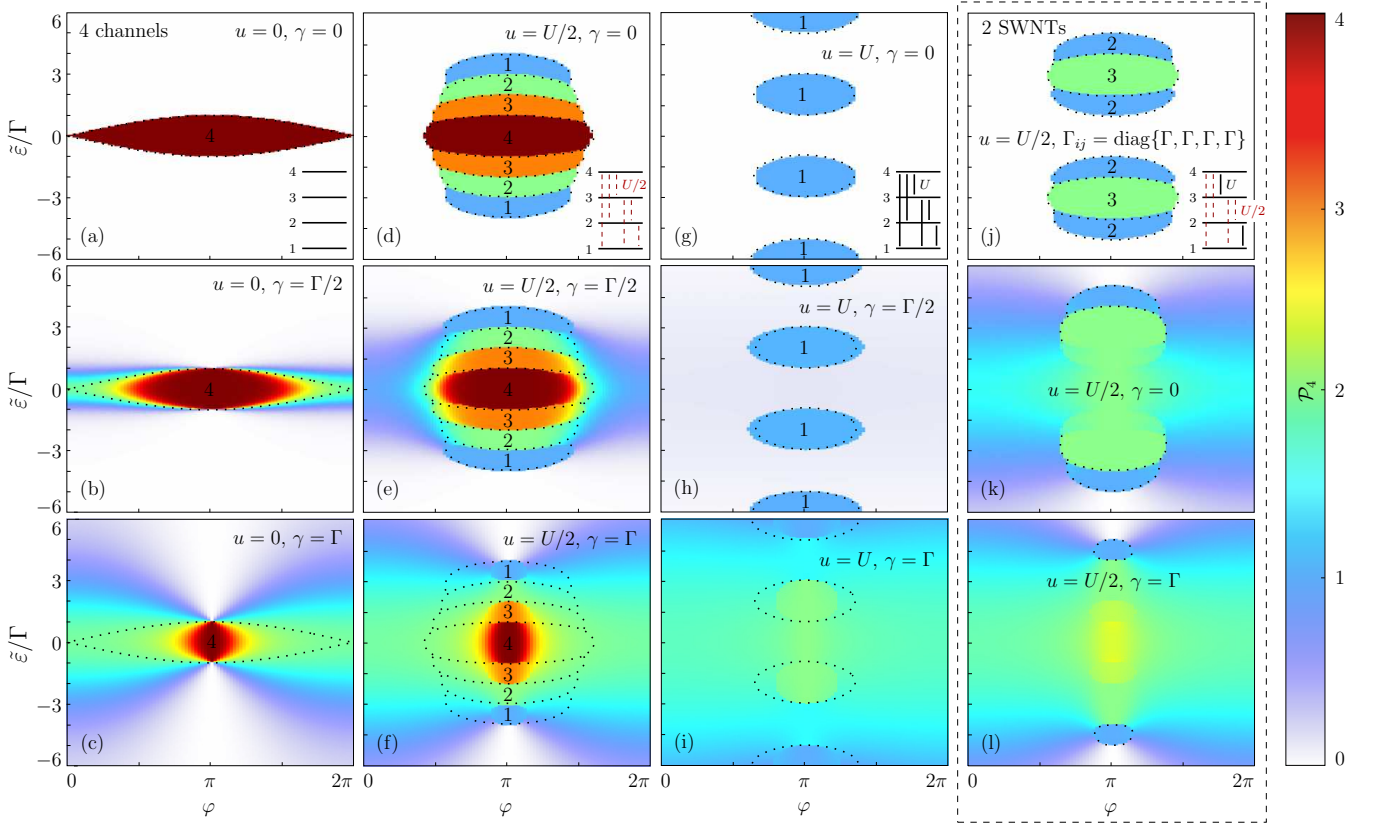$$U_{ij} = \begin{cases} U, & i = j, \\ u, & i \neq j. \end{cases} \tag{16}$$

FIG. 7: System degeneracy $\mathcal{P}_4$ of the ground state for $N = 4$ channels. (a)-(c) $\mathcal{P}_4$ goes from 0 to 4 in a step-like manner for $\gamma = 0$ and smoothly for $\gamma > 0$ [compare with Figs. 4(a)-4(c) and 6(a)-6(c)]; the Coulomb matrix U_{ij} is defined by Eq. (16) and the AR Γ_{ij} is defined by Eq. (17). (d)-(f) The average Coulomb interaction between channels $u = U/2$ transforms the $\mathcal{P}_4 = 4$ region to $\mathcal{P}_4 = 1$, 2, 3, and 4 regions [compare with Figs. 4(g)-4(i) and 6(d)-6(f)]. (g)-(i) The maximal Coulomb interaction between channels $u = U$ splits the $\mathcal{P}_4 = 4$ region to 4 regions with $\mathcal{P}_4 = 1$ at a distance $4u$ [compare with Figs. 4(j)-4(l) and 6(g)-6(i)]. (j) Two parallel SWNT: U_{ij} is defined by Eq. (19), Γ_{ij} by Eq. (17) with $\gamma = 0$. The structure is similar to the double structure in Fig. 4(g). (k) and (l) Two SWNT: U_{ij} defined by Eq. (19), Γ_{ij} by Eq. (20) for $\gamma = 0$ and $\gamma = \Gamma$.

Here U is the interaction within each channel and u is the interaction between any pair of channels, with $u \leqslant U$. The Coulomb interaction Eq. (16) describes N parallel wires, each with one channel (no orbital degeneracy). In this model the coupling to the superconductor is given by the matrix

$$\Gamma_{ij} = \begin{cases} \Gamma, & i = j, \\ \gamma, & i \neq j. \end{cases} \quad (17)$$

The diagonal elements Γ correspond to the regular Andreev reflection and off-diagonal elements γ describe crossed Andreev reflection (CAR). The situation $\gamma < \Gamma$ is possible, e.g., in the fork geometry shown in Fig. 5.

The results of the numerical calculation for $\varepsilon_1 = \varepsilon_2 = \ldots = \varepsilon_N$ and $U = \Gamma$ are presented in Figs. 4(a)-4(c) and 4(g)-4(l) [$N = 2$] as well as Figs. 6 [$N = 3$] and Figs. 7(a)-7(i). Here $\tilde{\varepsilon} = \varepsilon_1 + 2U + 2(N-1)u$.

In the absence of Coulomb interaction between channels, $u = 0$, and zero CAR $\gamma = 0$, the channel contributions are additive and the system is either in the non-degenerate state $\mathcal{P}_N = 0$ or in the state with $\mathcal{P}_N = N$ and degeneracy $2^{\mathcal{P}_N}$, see Figs. 4(a), 6(a), and 7(a). A nonzero γ leads to smearing of the borders between $\mathcal{P}_N = 0$ and $\mathcal{P}_N = N$ regions, see Figs. 4(b), 6(b), and 7(b) for $\gamma = 0.1\Gamma$ and Figs. 4(c), 6(c), and 7(c) for $\gamma = \Gamma$.

For $0 < u < U$ and $\gamma = 0$, the areas with integer $\mathcal{P}_N = 0, 1, \ldots, N$ are shown in Figs. 4(g), 6(d), and 7(d). The "centers" of the regions with $\mathcal{P}_N > 0$ are separated by distances defined by the off-diagonal elements of U_{ij}, e.g., for Eq. (16) these distances are $4u$. Nonzero values of γ result in continuous $\mathcal{P}_N$ in $[0 \ldots N]$, see Figs. 4(h)-4(i), 6(e)-6(f), and 7(e)-7(f).

For $u = U$ and $\gamma = 0$ there are N regions separated by $4u$ with $\mathcal{P}_N = 1$ [Figs. 4(j), 6(g), and 7(g)]. CAR $\gamma > 0$ increases $\mathcal{P}_N$ in regions which were zero initially at $\gamma = 0$; $\mathcal{P}_N$ can be increased as well as decreased from 1 [Figs. 4(k)-4(l), 6(h)-6(i), and 7(h)-7(i)].

B. Nanotubes

In this section, we describe Andreev quantum dots based on a single-wall nanotube, two parallel single-wall

nanotubes [Fig. 2(b)], or multi-wall nanotube/molecule [Fig. 2(c)].

The single-wall nanotube specifies a 2-channel Coulomb matrix and an Andreev reflection matrix

$$U_{ij} = \begin{bmatrix} U & U \\ U & U \end{bmatrix}, \quad \Gamma_{ij} = \begin{bmatrix} \Gamma & \Gamma \\ \Gamma & \Gamma \end{bmatrix}. \qquad (18)$$

The existence of two orbital states leads to the appearance of two doubly degenerate regions, see Fig. 4(l).

Two parallel single-wall nanotubes can be described by the Coulomb matrix

$$U_{ij} = \begin{bmatrix} U & U & u & u \\ U & U & u & u \\ u & u & U & U \\ u & u & U & U \end{bmatrix} \qquad (19)$$

and an AR matrix

$$\Gamma_{ij} = \begin{bmatrix} \Gamma & \Gamma & \gamma & \gamma \\ \Gamma & \Gamma & \gamma & \gamma \\ \gamma & \gamma & \Gamma & \Gamma \\ \gamma & \gamma & \Gamma & \Gamma \end{bmatrix}. \qquad (20)$$

The 2×2 block structure appears due to the twofold orbital degeneracy in the single-wall nanotube, where u and γ describe the interaction between nanotubes. The structure of the ground state for $\gamma = 0$ is presented in Fig. 7(j): both regions with $\mathcal{P}_N = 1$ (two-fold degeneracy) and $\mathcal{P}_N = 2$ (four-fold degeneracy) are present. Two "copies" of 1-2-1 regions appear due to orbital degeneracy in each nanotube, which can be compared to Fig. 4(g) for the case with no orbital degeneracy. In Figs. 7(k) and 7(l) the $\mathcal{P}_N$ behavior at $\gamma = 0.1\Gamma$ and $\gamma = \Gamma$ is shown.

The multi-wall nanotube has four or more orbital states. The most simple case $N = 4$ can be described by the interaction matrix Eq. (19) with $u = U$ [or the same Eq. (16)]. This situation is illustrated in Figs. 7(g)-7(i).

In the case of a diagonal Γ_{ij} ($\Gamma_{ij} = 0$, $i \neq j$) the ground state is created from the singlet $|0\rangle$, $|2\rangle$ or doublet $|\uparrow\rangle$, $|\downarrow\rangle$ states (but not a mixture of singlet and doublet states of the same channel) and $\mathcal{P}_N$ takes on integer values only. In the case of arbitrary off-diagonal elements Γ_{ij} ($\Gamma_{ij} \geqslant 0$, $i \neq j$) the ground state can be a mixture of all possible states including simultaneously $|0\rangle$, $|\uparrow\rangle$, $|\downarrow\rangle$, and $|2\rangle$ states from the same channel.

The value of $\mathcal{P}_N$ has a large impact on the physical properties of the dot, such as magnetic properties, charge on the dot, and the Josephson current.

VI.   MAGNETIC PROPERTIES

In this section, we describe the magnetic properties of the ground state in the presence of a weak external magnetic field. We take into account only the Zeeman splitting and neglect all other lower-order effects such as Rashba spin-orbit coupling (see Ref. 25 for more details).

This situation can be described by an additional term to the Hamiltonian (4) with a magnetic field B in the transverse direction

$$\hat{\mathcal{H}}_{\mathrm{M}} = \frac{g\mu_{\mathrm{B}}B}{\hbar} \sum_{i=1}^{N} \sum_{\sigma} s_\sigma \hat{n}_{i\sigma}, \qquad (21)$$

where $g \approx 2$ is the Landé factor and $\mu_{\mathrm{B}} = |e|\hbar/2m$ the Bohr magneton. The spin quantum number is $s_{\downarrow/\uparrow} = \mp\hbar/2$ in the corresponding i^{th} channel. In the presence of a magnetic field, the doublet state of each channel splits into two levels with energy difference $g\mu_{\mathrm{B}}B$.

In the absence of CAR, $\mathcal{P}_N$ takes on only the integer values from 0 to N. Then, the lowest level of the system with spin $-\mathcal{P}_N/2$ (where $\mathcal{P}_N$ is the number of channels in this doublet state) is non-degenerate, the first excited with spin $-(\mathcal{P}_N - 2)/2$ is $\mathcal{P}_N$-degenerate, etc. The whole picture is presented in the Table I. In this table $C_{\mathcal{P}_N}^i \equiv \mathcal{P}_N!/(\mathcal{P}_N - i)!\,i!$ and naturally $\sum_{i=0}^{\mathcal{P}_N} C_{\mathcal{P}_N}^i = 2^{\mathcal{P}_N}$. The magnetic properties of the system corresponds to a

TABLE I: The spins and degeneracies of the states obtained from a $2^{\mathcal{P}_N}$ degenerate ground state with Zeeman splitting.

State	Spin	Degeneracy
$\uparrow\uparrow \ldots \uparrow\uparrow$	$\mathcal{P}_N/2$	$C_{\mathcal{P}_N}^{\mathcal{P}_N} = 1$
$\uparrow\uparrow \ldots \uparrow\downarrow$	$\mathcal{P}_N/2 - 1$	$C_{\mathcal{P}_N}^{\mathcal{P}-1} = \mathcal{P}_N$
$\ldots$	$\ldots$	$\ldots$
$\uparrow\uparrow \ldots \downarrow\downarrow$	$-\mathcal{P}_N/2 + i$	$C_{\mathcal{P}_N}^i$
$\ldots$	$\ldots$	$\ldots$
$\uparrow\downarrow \ldots \downarrow\downarrow$	$-\mathcal{P}_N/2 + 1$	$C_{\mathcal{P}_N}^1 = \mathcal{P}_N$
$\downarrow\downarrow \ldots \downarrow\downarrow$	$-\mathcal{P}_N/2$	$C_{\mathcal{P}_N}^0 = 1$

system of $\mathcal{P}_N$ independent spins $1/2$. The influence of the Hamiltonian (21) leads to a change in size of the degenerate regions, which is equivalent to changing the Coulomb interaction U. The dependence of $\mathcal{P}_N$ on φ and $\tilde{\varepsilon}$ has been discussed in Sec. V.

VII.   CHARGE AND JOSEPHSON CURRENT

The operator for the total dot charge is given by

$$\hat{\mathcal{Q}}_N = \sum_{i=1}^{N} \mathbb{1}_1 \otimes \ldots \otimes \hat{Q}_i \otimes \ldots \otimes \mathbb{1}_N, \qquad (22)$$

where $\hat{Q}_i = e\hat{n}_i = e\,(\hat{d}_{i\uparrow}^\dagger \hat{d}_{i\uparrow} + \hat{d}_{i\downarrow}^\dagger \hat{d}_{i\downarrow})$ is the ith channel charge operator. The latter has matrix elements $Q_i = e\,\mathrm{diag}_i\{0, 1, 1, 2\}$. The dot charge (22) has matrix elements
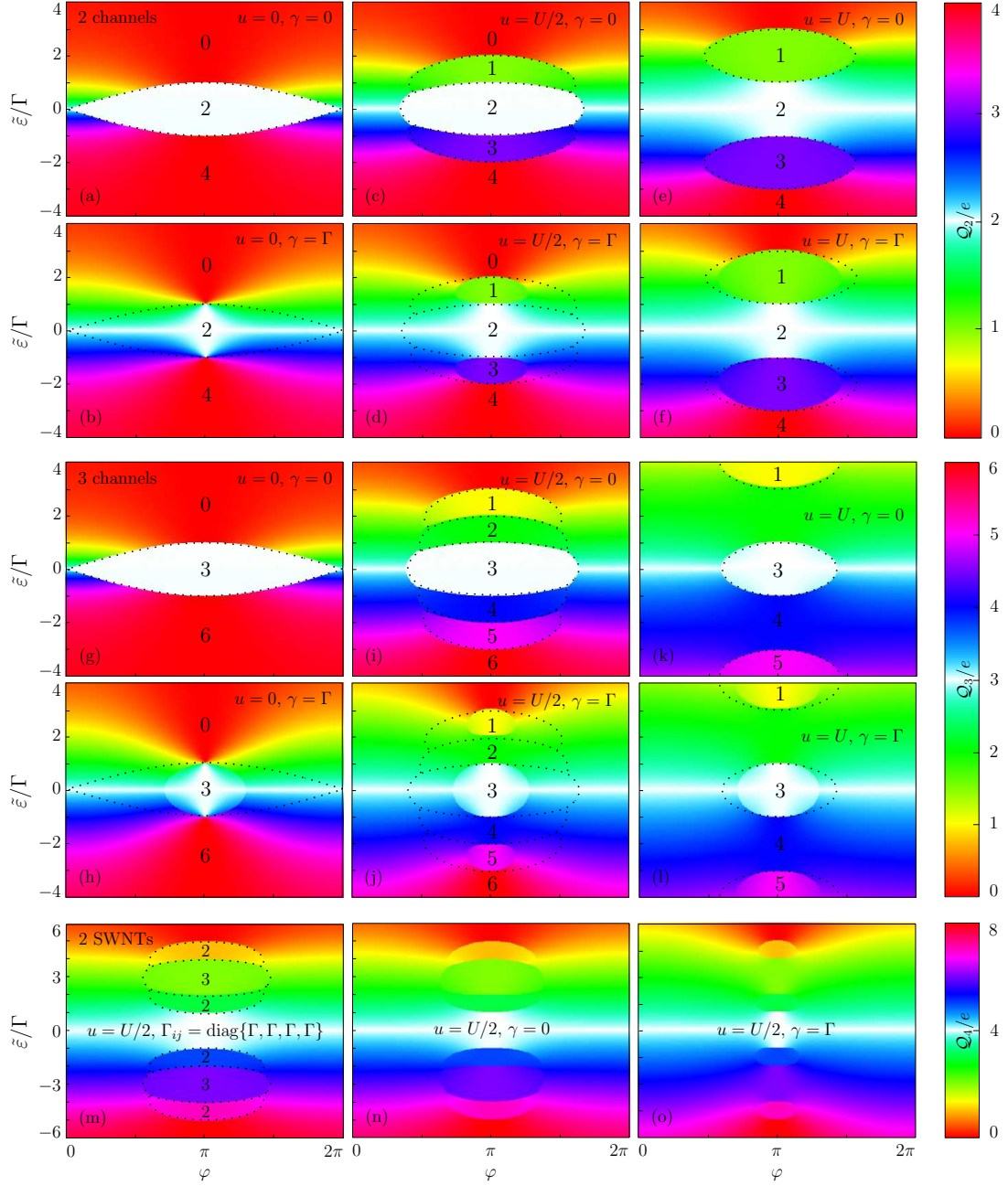
$$\mathcal{Q}_N = e \sum_{i=1}^{N} n_i, \qquad (23)$$

FIG. 8: Charge of the ground state $\mathcal{Q}_{2,3,4}$ in $(\varphi, \tilde{\varepsilon})$ space. Plots (a)-(f) [$N = 2$], (g)-(l) [$N = 3$] are for U_{ij} and Γ_{ij} as defined by Eqs. (16) and (17). Plot (m) corresponds to the two nanotubes [U_{ij} defined by Eq. (19)] and zero CAR between all channels [Eq. (17)]. Plots (n) and (o) describe two nanotubes [U_{ij} and Γ_{ij} are given by Eqs. (19) and (20)] with suppressed and maximal CAR between nanotubes. In all plots the charges goes from 0 (cold red) to $2Ne$ (warm red); the "centralized" charge Ne is shown in white color. Note that for all different N there are different colorbars.

where the matrices n_i are inserted using the same rules as in formula (13).

The charge of the ground state is presented in Fig. 8 as a function of φ and $\tilde{\varepsilon}$. In each channel, the charge can vary from $2e$ to 0 when increasing $\tilde{\varepsilon}$; the Coulomb interaction u and crossed Andreev reflections γ changes the total charge from the straightforward sum of channels charges.

In the single channel case $N = 1$ the charge $\mathcal{Q}_1$ can vary from 0 to $2e$; for the diagonal U and Γ matrices [Eqs. (16) and (17)] the total charge $\mathcal{Q}_{2,3}$ is reduced to the sum of charges from each channels as shown for $N = 2$ in Fig. 8(a) and for $N = 3$ in Fig. 8(g). The white flat plateau in the middle part of the plot corresponds to the region with $\mathcal{P}_N = N$ and $\mathcal{Q}_N = eN$; in this region, the charge does not depend on φ or $\tilde{\varepsilon}$.[10,22] The nonzero u "di-
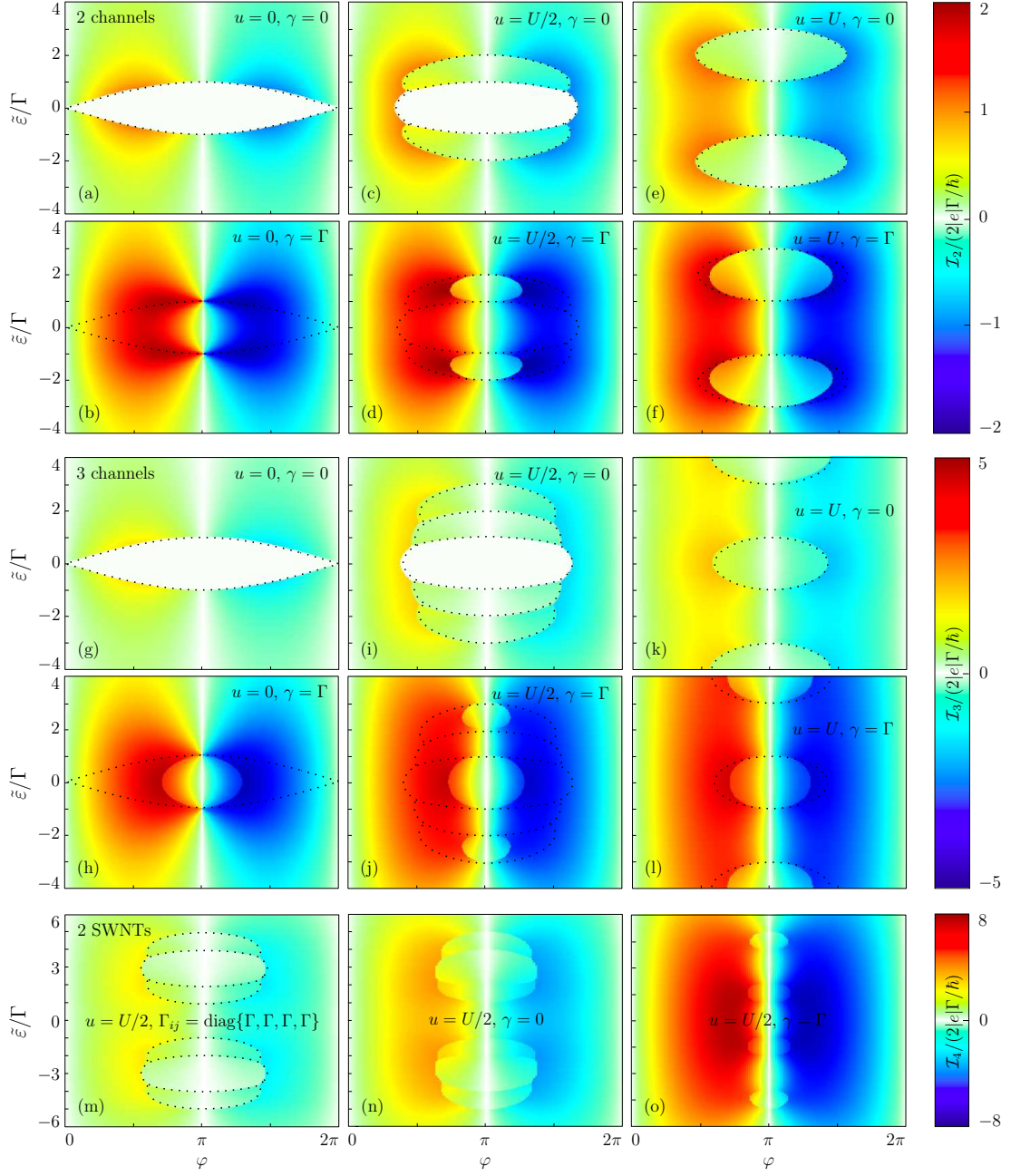
FIG. 9: The Josephson current of the ground state $\mathcal{I}_{2,3,4}$ in $(\varphi, \tilde{\varepsilon})$ space. All parameters are the same as in Fig. 8. A zero current is depicted by white color, negative by blue, and positive by red. For all $N = 2, 3, 4$ there are different colorbars.

vides" this region into pieces: partially [e.g. Figs. 8(c) and 8(i)] or fully [e.g. Figs. 8(e) and 8(k)]. In the regions with $\mathcal{P}_N < N$ only charges from $N - \mathcal{P}_N$ channels contribute to the phase dependent part of the total charge; the remaining channels ($\mathcal{P}_N$) give a constant contribution e. As previously, CAR smears the borders of the plateau as shown in Figs. 8(b)-8(f) and 8(h)-8(l). In Figs. 8(m)-8(o) the total charge $\mathcal{Q}_4$ of the two SWNTs connected in parallel is presented; for comparison see Figs. 7(j)-7(l) with $\mathcal{P}_4$. The charge in each channel is changed from 0 to $2e$, so the total charge goes from 0 to $2eN$. The scaling of

the phase-dependent part of the charge will be analyzed in Sec. VIII.

The total Josephson current operator is given by the expression

$$\hat{\mathcal{I}}_N = \sum_{i=1}^{N} \mathbb{1}_1 \otimes \ldots \otimes \hat{I}_i \otimes \ldots \otimes \mathbb{1}_N, \qquad (24)$$

where

$$\hat{I}_i = -\frac{2e}{\hbar} \Gamma_i \sin \frac{\varphi}{2} (\hat{d}_{i\downarrow} \hat{d}_{i\uparrow} + \hat{d}_{i\uparrow}^\dagger \hat{d}_{i\downarrow}^\dagger) \qquad (25)$$

is the ith channel current operator. The latter has matrix elements

$$I_i = -\frac{2e}{\hbar}\,\Gamma_i \sin\frac{\varphi}{2}\,\text{adiag}_i\{1,0,0,1\}. \qquad (26)$$

The total current operator can be generated in the same way as in Eqs. (13) and (23). Note that the charge $\hat{\mathcal{I}}_N$ and current $\hat{\mathcal{I}}_N$ can be obtained as a derivate with respect to V_{g} and φ, respectively. The Josephson current $\mathcal{I}_N$ corresponding to the operator (24) is presented in Fig. 9 as a function of the superconducting phase difference φ and $\tilde{\varepsilon}$.

In the non-interacting case $u = 0$ and $\gamma = 0$, the current is defined by energy the levels Eqs. (8) and (9) and scales proportional to the number of channels N, see Fig. 9(a) for $N = 2$ and in Fig. 9(g) for $N = 3$. The white region corresponds to the zero-current region; along the horizontal lines the current demonstrates the usual sine behavior (if the channel is in the singlet state) or zero current behavior (if the channel is in the doublet state).[9,22] In the maximally degenerate regions $\mathcal{P}_N = N$ the current can flow in the opposite direction (π-junction) if the continuous spectrum above Δ is taken into account.[9,26–29] The channels can be in the doublet state simultaneously [Figs. 9(a) and 9(g)] or asynchronously [Figs. 9(c), 9(e), 9(i), and 9(k)]. The small CAR γ smears the borders of the degenerate regions [Figs. 9(b), 9(d), and 9(f)], large CAR decreases or even eliminates the degenerate regions [Figs. 9(h), 9(j), and 9(l)].

The total current through two parallel SWNTs is shown in Figs. 9(m)-9(o); for comparison see Figs. 7(j)-7(l).

The Coulomb interaction as usually suppresses the current; CAR adds additional $N(N-1)$ channels for the current and therefore increases the current. Note that in the limits considered here, the maximal $\mathcal{P}_N = N$ leads to zero charge and current response with respect to φ; with decreasing $\mathcal{P}_N$ the response increases.

VIII. SENSITIVITY

Let us now analyze the sensitivity of the charge $\mathcal{Q}$ with the superconducting phase difference φ. The most relevant physical quantity is the differential sensitivity $\mathcal{S} = (4e/\hbar)\partial_\varphi\mathcal{Q}$. It characterizes the charge response to infinitely small deviations of the superconducting phase and describes the operating component in new types of magnetometers based on the charge of the Andreev quantum dot proposed in Refs. 10,22. The above defined sensitivity coincides with the current-to-gate voltage sensitivity $\tilde{\mathcal{S}} = e\,\partial\mathcal{I}/\partial\tilde{\varepsilon}$, which characterizes the Josephson transistor.[18] This correspondence can easily be proven if we remember that the charge is the energy derivative with respect to the gate voltage and the current is the energy derivative with respect to the phase. This implies that the results we find for the differential sensitivity of the magnetometer are also true for the sensitivity of the Josephson transistor. We will denote $\mathcal{S}_N$ as the sensitivity of the system with N channels.

The sensitivity as a function of the phase difference φ and the gate voltage $\tilde{\varepsilon}$ is displayed in Fig. 10. Given the case of multiple channels and the absence of Coulomb interaction between them, it is natural to expect the sensitivity to be composed from the sensitivity of each channel separately as shown in Fig. 10(a) and in Fig. 10(g). In this section we examine the influence of the Coulomb interaction between channels and CAR on the sensitivity.

Due to the slow singlet-doublet transitions we analyze only the sensitivity which comes from the channels in the singlet regime and omit the sensitivity given by the step in the charge during the singlet-doublet transition: for low frequency measurements this kind of sensitivity may be quite important.

In the absence of the Coulomb interaction $u = U = 0$ and the same normal dot levels $\varepsilon_1 = \varepsilon_2 = \ldots = \varepsilon_N$ the differential sensitivity has a maximum near point $\varphi = \pi$ and $\tilde{\varepsilon} = \varepsilon_1 = 0$.[10]

In case of a single channel $N = 1$ with Coulomb interaction $U = \Gamma$, the charge at $\varphi = 0$ and $\varphi = \pi$ is insensitive to the phase. The maximal sensitivity appears at the border of the doublet region. See the shape Fig. 10(a) for $N = 2$ and Fig. 10(g) for $N = 3$.

If we consider the two-channel case $N = 2$ with different dot levels $\varepsilon_1 \neq \varepsilon_2$ without the Coulomb interaction $u = U = 0$, then the sensitivity is defined by the distance $\delta\varepsilon_{12} = \varepsilon_2 - \varepsilon_1$. If this distance equals to zero, then the sensitivity $\mathcal{S}_2 = 2\mathcal{S}_1$. With increasing $|\delta\varepsilon_{12}|$ the sensitivities associated with different channels are canceled inside the region $[\varepsilon_1 \ldots \varepsilon_2]$ due to the different signs in the charge of the first and the second level and partially added outside this region. Given the large level separation $|\delta\varepsilon_{12}| \gg \Gamma$, the maximum sensitivity drops to the sensitivity of the single channel case $\mathcal{S}_2 = \mathcal{S}_1$.

The effects of the Coulomb interaction in the multichannel case $N > 1$ may be separated into the effect of degenerate regions ($0 < \mathcal{P}_N < N$ or $\mathcal{P}_N = N$) which are either partially or totally insensitive to the phase, and the effect of the repulsion between normal dots levels. Note that the size of the regions with $\mathcal{P}_N > 0$ decreases with increasing Coulomb interactions between levels, which can be seen by comparing Figs. 10(a), 10(c), and 10(e) or Figs. 10(g), 10(i), and 10(k). The combination of the normal level repulsion and the emergence of the insensitive regions leads to "oscillations" in the sensitivity as a function of φ and $\tilde{\varepsilon}$ as presented by the blue and red color in Fig. 10.

The sensitivity as shown in Figs. 10(b), 10(d), 10(f), 10(h), 10(j), and 10(l) can either increase or decrease due to the CAR. Partially, the CAR leads to a divergence in sensitivity at the points $(\varphi, \tilde{\varepsilon}) = (\pi, \pm\Gamma)$ in Figs. 10(b) and 10(h).

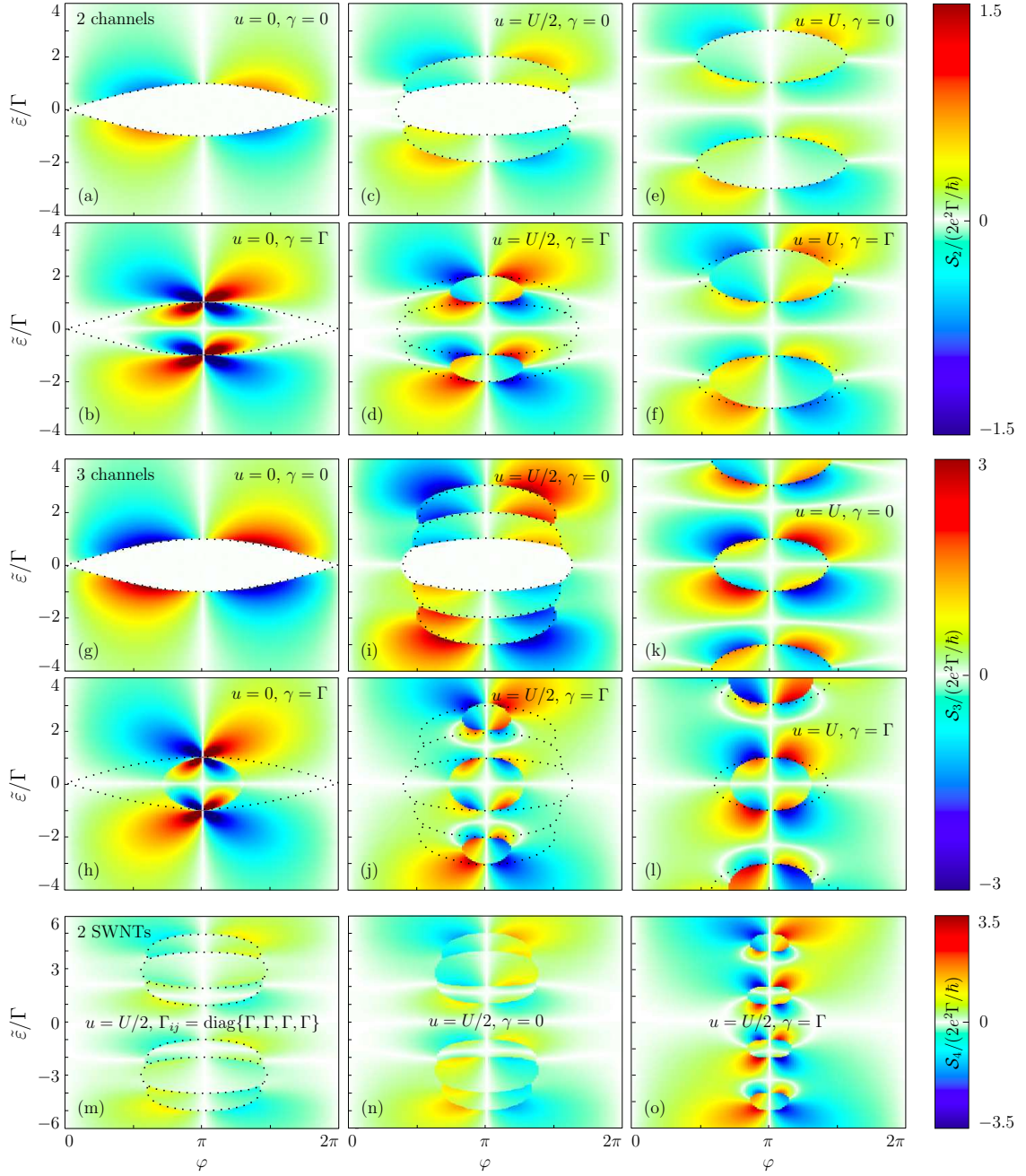The sensitivity of the two parallel SWNTs is shown in Figs. 10(m)-10(o).

FIG. 10: Charge-to-phase sensitivity in the ground state $\mathcal{I}_{2,3,4}$ in $(\varphi, \tilde{\varepsilon})$ space. All parameters coincide with Figs. 8 and 9. In the plots (b) and (h) the sensitivity diverges in $(\varphi, \tilde{\varepsilon}) = (\pi, \pm\Gamma)$ and sensitivity maximum (minimum) was cut by hands. For all N there are a different colorbars.

IX. CONCLUSION

In this article we have described an Andreev quantum dot with several normal levels/conducting channels in the infinite superconducting-gap limit. The scaling of the charge and the current with the number of channels is the central question of the work. We have introduced a recursive scheme for an N channel Hamiltonian and have analyzed it numerically/analytically.

This approach has allowed us to specify the degeneracy of the ground state, depending on the superconducting phase difference and the position of the back gate. Due to the Coulomb interaction inside each channel, doubly degenerate ground states appear. For the case of the intermediate Coulomb interaction between the channels, regions with a higher degeneracy are generated. Nevertheless, when increasing the Coulomb interaction between the channels, the doubly degenerate regions "repel" each other and regions with higher degeneracy disappear. The size of the doublet regions decrease due to

the Coulomb interaction between channels. The crossed Andreev reflection smears the borders between regions with different degeneracy and can destroy the regions with higher degeneracy at all. Also, we have studied the magnetic properties of the degenerate ground states in the presence of a Zeeman splitting.

Finally, the charge of the intermediate region and the current of the multi-channel Andreev dot have been computed. The interplay between the scaling and interaction effects has been discussed for some realistic situations. The charge-to-phase and current-to-gate voltage sensitivities increase with the number of channels but do not scale linearly as in the case of independent channels. While the sensitivity always increases with the number of channels, the Coulomb interaction between channels leads to a sensitivity reduction. A similar behavior has been detected for the critical current as a function of the number of channels. The multi-channel device could therefore be used as the sensitive magnetic flux detector or alternatively as the Josephson transistor. Summing up, the charge, the current, and the sensitivity scales linearly in the absence of crossed Andreev reflections and Coulomb interaction between channels. The Coulomb interaction suppresses the phase-dependent part and CAR smears the jumps as a function of phase difference and gate voltage.

[1] B.D. Josephson, Phys. Lett. **1**, 251 (1962).

[2] P.G. de Gennes, Rev. Mod. Phys. **36**, 225 (1964).

[3] P.W. Anderson and J.M. Rowell, Phys. Rev. Lett. **10**, 230 (1963).

[4] P. Jarillo-Herrero, J.A. van Dam, and L.P. Kouwenhoven, Nature **439**, 953 (2006).

[5] J.-P. Cleuziou, W. Wernsdorfer, V. Bouchiat, T. Ondarçuhu, and M. Monthioux, Nat. Nanotech. **1**, 53 (2006).

[6] N.M. Chtchelkatchev and Yu.V. Nazarov, Phys. Rev. Lett. **90**, 226806 (2003).

[7] I.A. Sadovskyy, G.B. Lesovik, and G. Blatter, Phys. Rev. B **75**, 195334 (2007).

[8] K. Engström and J. Kinaret, Phys. Scr. **70**, 326 (2004).

[9] A.V. Rozhkov and D.P. Arovas, Phys. Rev. B **62**, 6687 (2000).

[10] I.A. Sadovskyy, G.B. Lesovik, and G. Blatter, Pis'ma v ZhETF **86**, 239 (2007) [JETP Lett. **86**, 210 (2007)].

[11] R. Saito, G. Dresselhaus, and M.S. Dresselhaus, *Physical Properties of Carbon Nanotubes* (Imperial College Press, London, 1998).

[12] V.I. Falko and G.B. Lesovik, Solid State Comm. **84**, 835 (1992).

[13] A.F. Andreev, Zh. Eksp. Teor. Fiz. **46**, 1823 (1964) [Sov. Phys. JETP **19**, 1228 (1964)].

[14] G. Deutscher and D. Feinberg, Appl. Phys. Lett. **76**, 81 (2000).

[15] D. Beckmann, H.B. Weber, and H. v. Löhneysen, Phys. Rev. Lett. **93**, 197003 (2004).

[16] D. Beckmann and H. v. Löhneysen, AIP Conf. Proc. **850**, 875 (2006).

[17] G.B. Lesovik, T. Martin, and G. Blatter, Eur. Phys. J. B **24**, 287 (2001).

[18] D.D. Kuhn, N.M. Chtchelkatchev, G.B. Lesovik, and G. Blatter, Phys. Rev. B **63**, 054520 (2001).

[19] N.M. Chtchelkatchev, G.B. Lesovik, and G. Blatter, Phys. Rev. B **62**, 3559 (2000).

[20] L.D. Landau, E.M. Lifshitz, and L.P. Pitaevskii, *Electrodynamics of Continuous Media. Volume 8* (Butterworth-Heinemann, 1984).

[21] A. Zazunov, D. Feinberg, and T. Martin, Phys. Rev. Lett. **97**, 196801 (2006).

[22] I.A. Sadovskyy, G.B. Lesovik, T. Jonckheere, and T. Martin, Phys. Rev. B **82**, 235310 (2010).

[23] A. Martín-Rodero and A. Levy Yeyati, Adv. Phys. **60**, 899 (2011).

[24] B. Kubala and J. König, Phys. Rev. B **67**, 205303 (2003).

[25] Q.F. Sun, J. Wang, and H. Guo, Phys. Rev. B **71**, 165310 (2005).

[26] E. Vecino, A. Martín-Rodero, and A. Levy Yeyati, Phys. Rev. B **68** 035105 (2003).

[27] J.A. van Dam, Yu.V. Nazarov, E.P.A.M. Bakkers, S. De Franceschi, and L.P. Kouwenhoven, Nature **442**, 667 (2006).

[28] A. Zazunov, A. Schulz, and R. Egger, Phys. Rev. Lett. **102**, 047002 (2009).

[29] A. Zazunov, A. Levy Yeyati, and R. Egger, Phys. Rev. B **81**, 012502 (2010).